Naval Research Laboratory

Washington, DC 20375-5000

(2)

NRL/MR/6183—92-6994

Numerical Simulations of Spontaneous Ignition and Detonation in Propane-Air Mixtures

CAROLYN R. KAPLAN* AND ELAINE S. ORAN†

**Navy Technology Center for Safety and Survivability*
Chemistry Division

†Laboratory for Computational Physics and Fluid Dynamics

July 6, 1992

REPORT DOCUMENTATION PAGE

Form Approved
OMB No. 0704-0188

1. AGENCY USE ONLY (Leave blank)	2. REPORT DATE	3. REPORT TYPE AND DATES COVERED
	July 6, 1992	

4. TITLE AND SUBTITLE

Numerical Simulations of Spontaneous Ignition and Detonation in Propane-Air Mixtures

5. FUNDING NUMBERS

PE - 61153N
PR - 61-0087-F2

6. AUTHOR(S)

Carolyn R. Kaplan* and Elaine S. Oran†

7. PERFORMING ORGANIZATION NAME(S) AND ADDRESS(ES)

Naval Research Laboratory
Washington, DC 20375-5000

8. PERFORMING ORGANIZATION REPORT NUMBER

NRL/MR/6183—92-6994

9. SPONSORING/MONITORING AGENCY NAME(S) AND ADDRESS(ES)

Office of Naval Research
800 N. Quincy Street
Arlington, VA 22217

10. SPONSORING/MONITORING AGENCY REPORT NUMBER

11. SUPPLEMENTARY NOTES

*Navy Technology Center for Safety and Survivability, Chemistry Division
†Laboratory for Computational Physics and Fluid Dynamics

12a. DISTRIBUTION/AVAILABILITY STATEMENT

Approved for public release; distribution unlimited.

12b. DISTRIBUTION CODE

13. ABSTRACT (Maximum 200 words)

The spontaneous ignition and subsequent detonation of propane-air mixtures caused by a weak shock in a partially confined volume containing an obstacle are studied using time-dependent numerical simulations. The motivation for this work is two-fold: first, to examine potential hazards from a leaking storage container (an obstacle to the flow), and second, to study the fundamental interaction of a shock wave with an obstacle in an energetic ambient gas. The numerical model combines a solution of the compressible equations of fluid dynamics with a phenomenological chemical induction model for species conversion and energy release. Nonreactive simulations show how the obstacle partially blocks the flow such that one portion of the shock front reflects off of the obstacle and another portion is transmitted. Reactive-flow simulations of stoichiometric propane-air mixtures show spontaneous ignition behind the shock reflected from the obstacle and later transition to detonation in the direction of the transmitted wave. Computations performed to study the effect of obstacle height show that different physical mechanisms are responsible for the transition to detonation for the various obstacle sizes considered. Simulations in a mixture with variable stoichiometry around the obstacle, a more realistic picture of the physical scenario, show decay of the transmitted shock and then re-ignition as the shock reaches the stoichiometric region. Two separate areas of ignition eventually combine and transition to detonation. As this detonation propagates into the lean region far from the obstacle, it decays into a shock wave followed by a decaying flame front.

14. SUBJECT TERMS

Reactive-flow simulations
Spontaneous ignition
Transition to detonation

15. NUMBER OF PAGES

40

16. PRICE CODE

17. SECURITY CLASSIFICATION OF REPORT	18. SECURITY CLASSIFICATION OF THIS PAGE	19. SECURITY CLASSIFICATION OF ABSTRACT	20. LIMITATION OF ABSTRACT
UNCLASSIFIED	UNCLASSIFIED	UNCLASSIFIED	UL

CONTENTS

NUMERICAL SIMULATIONS OF SPONTANEOUS IGNITION AND DETONATION IN PROPANE-AIR MIXTURES

1. INTRODUCTION

Fires resulting from the accidental leakage of hydrocarbon fuels can have devastating consequences. Usually these leaks occur in confined environments where there are obstacles with complex shapes. The presence of obstacles will lead to an increase in the rate of burning and acceleration of the flame front, and, in many circumstances, may be responsible for producing violent explosions. Indeed, a wide variety of both large- and small-scale experimental tests have demonstrated the dramatic influence of confinement and the presence of obstacles on the severity of fuel-air explosions. Moen *et al.* (1986) have done experimental and numerical investigations of flame propagation for acetylene, propane and hydrogen sulfide fuels in a partially confined channel with an array of obstacles. Their results indicated that near-stoichiometric acetylene-air flames accelerate to speeds between 180 and 400 m/s before transitioning to detonation, while the less sensitive mixtures such as mixtures of lean acetylene, propane, and hydrogen sulfide in air showed much less dramatic behavior. The study concluded that the potential for flame acceleration and transition to detonation is much greater in heavily confined areas. Higher levels of confinement, stronger ignition sources, or more dense obstacle configurations are required to produce such explosions in less sensitive fuel-air mixtures. Laboratory-scale experiments by Urtiew *et al.* (1983) using a propane-air flame showed that the geometry of the partial confinement is of primary importance; obstacles cause acceleration of the flame front and cause faster burnout of the combustible vapor.

Results of large methane-air explosions (Moen *et al.* 1982) showed that even relatively small repeated obstacles have a dramatic influence on the violence of the explosion. Overpressures of 8.8×10^6 dynes/cm^2 were recorded in the confined areas containing obstacles, compared to 0.1×10^6 dynes/cm^2 in the chamber without obstacles. A theoretical study by Taylor (1986) has shown that the closely spaced obstacles trap large pockets of unburnt fuel behind the leading edge of the flame. As these pockets of fuel burn, they inject large quantities of burnt gas into the flow field, resulting in high steady-state flame speeds. The phenomenon is alleviated by allowing the gases to vent through a perforated plate (Chan *et al.* 1983).

Manuscript approved April 16, 1992.

The present work represents the beginning of our efforts to develop a comprehensive set of computational tools to model fire-hazard and explosion scenarios (Kaplan and Oran 1991-a,-b) of Naval interest. This report specifically describes a numerical study of spontaneous ignition of propane that has leaked from a storage container in a partially confined volume. The storage container itself serves as an obstacle which affects the severity of the resulting explosion. In this study, the ignition is caused by an incident shock wave, a condition that simulates a roof or wall collapsing, or a large piece of machinery or equipment falling down. On impact, there is a sudden pressure and density gradient in the background gas. Although the pressure and temperatures behind this wave are not high enough to cause immediate ignition, when this wave reflects from an obstacle, the temperatures and pressure increase again creating conditions where ignition is more likely to occur. In addition, the wave transmitted around the obstacle can cause ignition due to shock reflections and complex shock patterns formed on the wall boundaries. In this paper, we study the effects of the obstacle height, the strength of the incident shock wave, and the effects of variable stoichiometry of the fuel-air mixture around the obstacle. Although the scenario modeled here has been idealized to extract and study the basic physical interaction mechansims, comparisons made to related experimental work confirm a number of important trends and interaction mechanisms.

2. THE MODEL AND METHOD OF SOLUTION

2 a. Fluid Dynamics Model

The numerical simulation is based on the solutions of the compressible, time-dependent, conservation equations for total mass density ρ, momentum density $\rho\bar{v}$, and energy, E,

$$\frac{\partial \rho}{\partial t} = -\nabla \cdot \rho\bar{v} \qquad (1)$$

$$\frac{\partial \rho\bar{v}}{\partial t} = -\nabla \cdot (\rho\bar{v}\,\bar{v}) - \nabla P \qquad (2)$$

$$\frac{\partial E}{\partial t} = -\nabla \cdot (E\bar{v}) - \nabla \cdot (\bar{v}P) \qquad (3)$$

where $\bar{v}$ is the fluid velocity and P the pressure. In a multispecies fluid in which chemical reactions result in transformations among the species, we also need an equation for individual species number densities $\{n_i\}$,

$$\frac{\partial n_i}{\partial t} = -\nabla \cdot n_i\bar{v} + Q_i - L_i n_i , \qquad i = 1, \ldots, N_s \qquad (4)$$

where the $\{Q_i\}$ and $\{L_i\}$ are chemical production and loss terms, respectively, for species i. The effects of molecular diffusion, thermal conduction, and radiative diffusion have been omitted from these equations. The first two of these effects are generally insignificant on the time scales of interest for the present study and the last is not significant for the propane-air system discussed here. There is a constraint that defines the total number density, N,

$$N = \sum_{i=1}^{N_s} n_i \tag{5}$$

where N_s is the total number of different kinds of species present. The total energy is a sum of the kinetic and internal energy,

$$E = \frac{1}{2} \rho \bar{v} \cdot \bar{v} + e \tag{6}$$

where e is the specific internal energy.

An ideal-gas equation of state is used for the gas-phase calculations,

$$P = NkT = \rho RT \tag{7}$$

where k is the Boltzmann constant, R is the gas constant of the mixture, and T is the temperature of the gas. The relation between internal energy per unit volume, e, and pressure, P, for an ideal gas, is,

$$e = \frac{P}{\gamma - 1} \tag{8}$$

where γ is the ratio of specific heats.

2 b. Chemistry Model

In all of the calculations described here, the full details of the chemical reactions, that is, the complete set of $\{Q_i\}$ and $\{L_i\}$ describing the elementary reactions, are not included in the model. The large number of species and reactions involved, as well as uncertainties in the rates of elementary reactions, make it computationally impractical to include a detailed chemical reaction rate scheme in a complex multidimensional fluid dynamic problem such as the one discussed here. Instead, we use the induction parameter model that reproduces the essential features of the chemical reaction and energy release process. In this model, the induction time is calculated as a function of temperature and concentrations of propane and oxygen. Then a quantity called the induction parameter is defined and convected with the fluid in a Lagrangian manner. This parameter records the temperature history of a fluid element, and when the element is heated

long enough, energy release is initiated.

In general, the induction parameter model for representing the properties of a chemical reaction mechanism in a numerical simulation is valid for fast flows in which the convective timescales are significantly faster than those for physical diffusion. The input quantites, such as induction time, final temperature, and energy release rate, may be derived from experimental data, as in this study, or they may also be obtained by integrating the full set of elementary chemical reactions and tabulating these quantities as a function of temperature and pressure. The model was described originally by Oran *et al.* (1981) and has been developed further by Kailasanath *et al.* (1985) and Guirguis *et al.* (1986, 1987).

In the induction parameter model, the combustion of a premixed propane-air mixture proceeds by a simplified two-step parametric model. During the first step, the reactants break up and intermediate radicals are formed, but because there is not yet any substantial energy release, the mixture remains essentially thermoneutral. During this induction step, the reactions taking place are modeled by

$$\textit{fuel} + \textit{oxidizer}\ (+\ \textit{diluents}) \rightarrow \textit{radicals}\ (+\ \textit{diluents}) \qquad (9)$$

The second step models the energy-release process, which is the time of rapid reactions and formation of stable products that starts after the induction time has elapsed. During the energy release step, the reactions taking place are modeled by

$$\textit{fuel} + \textit{oxidizer} + \textit{radicals}\ (+\textit{diluents}) \rightarrow \textit{products}\ (+\ \textit{diluents}) \qquad (10)$$

In many combustion systems, both steps occur simultaneously after the first step has been initiated. However, during the induction step, the change in concentrations and the amount of energy released are small enough that they can be neglected in a simplified model. Thus the temperature and pressure are held constant during the induction period. This simplification enables us to use the chemical induction time data which are usually available at constant temperatures and pressures for mixtures of specified stoichiometry.

The time corresponding to the first step, the chemical induction period, τ_i, has been fit to an analytical expression by Burcat *et al.* (1971) based on their experimental data

$$\tau_i = 4.4x10^{-14} \exp\left[(42.2x10^3/RT)\right] [Ar]^0\ [C_3H_8]^{0.57}\ [O_2]^{-1.22} \qquad (11)$$

where the concentrations are in moles/cc, [Ar] is Argon concentration and τ is in seconds. Then the quantity f, denoting the fraction of the chemical induction time elapsed at time t, may be found from

$$\frac{df}{dt} = \frac{1}{\tau_i} \qquad (12)$$

In the second step, reactants are converted to products according to the finite reaction rate,

$$\frac{d\rho_f}{dt} = -(\rho_f)\, A_r \exp\,(-E_r/RT) \qquad (13)$$

where ρ_f is the concentration of fuel, A_r is the pre-exponential factor, and E_r is the activation energy. During this energy release step, we assume that the activation energy is small, $E_r \sim 0$.

To complete the parametric model, we define the value of the final concentration of the fuel, which is obtained from equilibrium calculations (Gordon and McBride 1976). Specification of the final concentration of the fuel determines the amount of energy released. The temperature of the reacted material is 2000 K.

2 c. Numerical Method of Solution

The convective transport equations, those parts of Eqs. (1) - (4) excluding the chemical reaction terms, are rewritten in terms of finite-difference approximations on an Eulerian grid. The mass density, momentum, and total energy are convected using the nonlinear, fully compressible, flux corrected transport (FCT) algorithm (Boris and Book 1976), LCPFCT (Oran and Boris 1987, Boris *et al.* 1992). FCT is an explicit, finite-difference algorithm with fourth-order phase accuracy and is designed to ensure that all conserved quantites remain monotonic and positive. The procedure for using this one-dimensional algorithm with direction and timestep splitting to produce two-dimensional or three-dimensional solutions is described in some detail by Oran and Boris (1987). Those parts of the coupled set of equations that describe the chemical reactions, Eqs. (12) and (13), are solved analytically. The chemical reaction model is treated as a source term in the FCT algorithm. These results are combined with the FCT solutions for the convective transport by timestep splitting methods, as discussed by Oran and Boris (1987).

3. THE PHYSICAL PROBLEM

Simulations were conducted on a two-dimensional Cartesian grid with 200 cells in the x-direction and 30 cells in the y-direction. In addition, resolution tests were conducted on a grid with exactly double resolution to ensure that the grid provided adequate resolution of the structure. The computational domain is shown in Figure 1. The grid spacing was uniform with $\delta x = \delta y = 0.5$ cm. The obstacle was located at cell 50 along the x-axis, and is five cells (2.5 cm) wide and 15 cells (7.5 cm) high. Timesteps used in the simulations are on the order of 1×10^{-6} s. At the

beginning of the computation, the inflow gas enters the computational domain from the left side, while the background gas is initially stationary. The inflow boundary condition (Boris *et al.* 1992) specifies the density, temperature, pressure, and velocity of the inflowing gas, which are determined from the normal shock relations for an ideal planar shock. The right-hand side of the computational domain boundary has an extrapolated outflow boundary condition (Boris *et al.* 1992), which ensures that the fluid properties do not change between the last cell inside the computational domain and the guard-cell outside the domain. The top and bottom boundaries are solid walls, represented by free-slip boundary conditions (Boris *et al.* 1992).

Table I lists the scenarios for which simulations were conducted, where M is the Mach number of the incident planar shock wave and ϕ is the equivalence ratio. Case A is a nonreactive simulation for air and shows the flow resulting from the reflection of a shock wave off of an obstacle. Case B-1 is a reactive simulation, in which both the inflow and background gases are stoichiometric propane-air mixtures. This simulation corresponds to the case in which the propane has leaked from the container and uniformly diffused throughout the simulated volume. Cases B-2 and B-3 are identical to case B-1 except that the obstacle height was varied to quantify the effect of obstacle size on the resulting detonation or fire hazard. Case C simulations are the same as case B-1, except that the incident shock wave is stronger (C-1) and weaker (C-2). Case D is a variable stoichiometry simulation in which the inflowing gas is air, while the background gas is fuel-rich in the area immediately surrounding the obstacle and

Table I. Listing of simulations conducted.

Case	Inflow material	Ambient gas	Obstacle height (cm)
A	air, M = 1.34	air, STP	7.5
B-1	propane-air, $\phi = 1$, M = 1.34	propane-air, $\phi = 1$, STP	7.5
B-2	propane-air, $\phi = 1$, M = 1.34	propane-air, $\phi = 1$, STP	3.5
B-3	propane-air, $\phi = 1$, M = 1.34	propane-air, $\phi = 1$, STP	11.5
C-1	propane-air, $\phi = 1$, M = 1.40	propane-air, $\phi = 1$, STP	7.5
C-2	propane-air, $\phi = 1$, M = 1.31	propane-air, $\phi = 1$, STP	7.5
D	air, M = 1.34	propane-air, ϕ variable, STP	7.5

becomes progressively leaner with distance from the obstacle. This last case represents the scenario in which the fuel has leaked from the container, but has not yet diffused throughout the entire volume, so that the fuel concentration surrounding the container is rich ($\phi=2$) and decreases linearly with distance from the container to $\phi=0.5$ at the end of the computational domain. In all cases, the ambient background gas is at standard conditions, $1.01\text{x}10^6$ dynes/cm^2 (1 atm) and 298 K.

4. RESULTS

Simulation results are presented as contours of variables such as pressure, temperature and species concentrations. In the following figures, the heavy thick contours correspond to steep gradients in the variables. The steep gradient can represent either the shock front or the reaction front, depending on which variable is contoured. For example, in the pressure contours, the thick dark lines represent a steep gradient in pressure and correspond to the location of the shock front. There will not be a steep pressure gradient across a flame front, hence, a reaction front representing a flame front cannot be seen in the pressure contours. However, if the flame has transitioned to a detonation, the steep pressure gradient due to the detonation will be shown in the pressure contours. The close heavy dark lines in the product concentration contours represent a steep gradient in the product concentration, and therefore represent the reaction front. The heavy dark lines in the temperature contours can correspond to either the shock front or the reaction front. The temperature contours show a steep gradient at the reaction front, since the temperature of the products is much greater than the temperature of the unreacted material. Temperature contours also show a steep gradient at the shock front, since the temperature of the incident shock is much greater than the temperature of the background gas. Therefore, the temperature contours must be simultaneously compared with the pressure contours (which show shock front) and product contours (which show reaction front) to determine which gradients represent the various fronts.

Case A: Nonreactive Case

Figure 2, the pressure contours for time steps 80 through 260, shows the basic structure that evolves as the planar, vertical shock passes over the obstacle. If there were no obstacle, the shock would continue unperturbed through the chamber, slowed only by viscous or thermal losses in the system. If the obstacle were the full height of the chamber, there would be a simple shock reflection of the type used in standard shock-tube kinetics experiments. However, the presence

of the obstacle partially blocks the flow and dramatically changes the flow both qualitatively and quantitatively.

At step 80, the shock front has just reached the obstacle surface. By step 100, the lower half of the shock front has reflected from the obstacle producing a Mach 2.0 reflected shock. The reflected shock wave moves both upstream (toward the left) and expands upward into the region above the obstacle by step 140. The temperature of the gas behind the reflected shock is 1350°K, but decreases in the region above the obstacle as the fluid expands and cools. The reflected, upward expanding shock reaches the top boundary (solid wall) by step 220, and there is a Mach reflection at this upper wall.

The upper half of the incident shock is transmitted over the obstacle and has cleared it by step 140. This transmitted shock expands while travelling downstream (toward the right) and reaches the lower boundary solid wall by step 220. By step 260, the transmitted shock forms a Mach reflection at the lower boundary wall.

Case B-1: Stoichiometric Propane-Air Mixture

Figures 3, 4, 5, and 6 show pressure, product, fuel and temperature contours, respectively, for timesteps 100-280, for Case B-1, which has the same configuration as Case A, but where the mixture is now propane and air that react chemically under the appropriate conditions. As in Case A, the lower half of the incident shock front has reflected from the obstacle surface by step 100. The maximum temperature behind the reflected shock is 1350 K, which corresponds to a chemical induction time of 30×10^{-6} s. Thus by step 130, energy release has begun in the reflected shock region and products have begun to form. As shown in Figure 4, at timestep 140, chemical reactions start very close to the obstacle behind the reflected shock. Comparing pressure (Fig. 3) contours to product (Fig. 4) contours shows that the reaction wave is closely coupled to the reflected shock front. By timestep 180, the reaction wave behind the obstacle has caught up with the reflected shock front, resulting in a curved detonation propagating upstream (toward the left).

As shown in Fig. 3, this detonation moving upstream expands upwards into the region above the obstacle and reflects from the upper boundary by timestep 220. The result is a detonation travelling upstream, another detonation travelling downstream (toward the right), and a shock wave that moves downward in reacted material towards the obstacle. At timestep 240, the pressure contours show a detonation travelling upstream and another detonation travelling downstream preceded by the transmitted shock. This detonation travelling downstream appears

as a curved detonation in the pressure contour at timestep 240. The shock wave that moves down towards the obstacle is attached to the curved detonation moving downstream into the unreacted propane-air mixture.

The downward-travelling shock wave reaches the lower boundary by timestep 280. When this shock reflects from the lower wall, the temperatures are raised and a reaction front is generated that is attached to the detonation travelling downstream by an oblique shock wave (shown in the product contours, Fig. 4, at timestep 280). This reaction front moves upstream to consume any unreacted propane and oxygen and also moves downstream with the attached detonation. Fuel contours (Fig. 5) show that the fuel is almost completely consumed in the region between the upstream- and downstream-travelling detonations. The detonation front moving downstream eventually overtakes the original transmitted shock.

When the original incident shock wave reflects from the obstacle, the expansion over the obstacle and flow behind the reflected shock bring hot product materials over the obstacle (shown in the product contours starting at timestep 200) so that the resulting shear causes the complex vortex shedding typical of flows over a step. This process is most clearly seen in the temperature contours, Fig. 6, starting at timestep 180, which show hot products passing over the obstacle. These vortical structures mix the unreacted fuel with the hot products. Then the shock wave that travels downward after reflecting from the upper wall interacts with the vortical structures which further enhances the chance of ignition in unreacted material near the lower bounding wall. This detailed interaction of a shock wave and a high-speed shear flow is beyond the scope and intent of this paper and would require much higher-resolution solutions to describe properly.

In summary, the results presented for Case B-1 show that two physical mechanisms contribute to the transition to detonation in the region downstream of the obstacle. The first is the reflection of the detonation from the top boundary (timestep 200), which in turn generates a detonation travelling downstream and a shock front travelling down towards the obstacle (timestep 240). The second mechanism is the formation of a reaction front near the lower boundary, either when the transmitted shock front reflects from this boundary or when the shock interacts with the shear flow (timestep 280). This reaction front then joins with the detonation front travelling downstream and eventually overtakes the original transmitted shock front.

Cases B-1, B-2, B-3: Effect of Obstacle Height

To determine the effect of obstacle size on the downstream transition to detonation, additional simulations were performed with obstacle heights of 3.5 cm and 11.5 cm, corresponding to Cases B-2 and B-3, respectively. Figure 7 shows the pressure contours at timesteps 180 and 260 for the three different obstacle sizes considered. Table II lists three times for each case: 1) the time when the detonation first reaches the top boundary, 2) the time when reactions start near the lower boundary, and 3) the time when there is a complete detonation (a detonation which extends completely from the top to the bottom boundary) downstream of the obstacle. The monotonic decrease of the first time in Table II (when the detonation reaches the top boundary) and increase of the second time (when reactions start near the lower boundary) appear consistent with the change in obstacle height. These trends follow from considering the differences in the times it takes for the detonation to reach the top wall and then for the reflected shock to reach the bottom wall downstream of the obstacle.

Consider the 7.5 cm obstacle. In this case, the detonation moving upstream reflects from the top boundary at timestep 200, and this generates the curved detonation front travelling downstream. Meanwhile, the transmitted shock that had passed the obstacle has reflected from the bottom boundary and ignited there by 280 timesteps. This reaction wave and the detonation front join together and form one detonation that overtakes the initial transmitted shock front by 300 timesteps.

Table II. Time when: 1) expanding detonation reflects from top boundary, 2) reaction wave forms at lower boundary, and 3) complete detonation forms downstream of obstacle.

Obstacle height (cm)	Effective blockage to forward flow (%)	Expanding detonation reflects off of top boundary (timesteps)	Formation of reaction wave at lower boundary (timesteps)	Transition to detonation ahead of obstacle (timesteps)
3.5	25	240	200	360
7.5	50	200	280	300
11.5	75	180	300	480

Table II shows that the reaction wave formed at the lower boundary occurs earliest for the 3.5 cm obstacle because the transmitted shock front has only a short distance to travel before it reflects from the lower boundary. However, the time required for the detonation moving upstream and expanding in the region above the obstacle to reflect off of the upper boundary is the longest for the 3.5 cm obstacle. This is because the reaction wave initially formed at the 3.5 cm obstacle surface is very short and takes a longer time to reach the upper boundary, as shown at timestep 180 in Figure 7. By timestep 260, this reaction wave has reached the upper boundary and generated a partial detonation (near the top boundary only) travelling downstream, but it is not as far downstream as for the 7.5 cm obstacle case. Therefore, the complete transition to detonation downstream occurs later for the 3.5 cm obstacle case than the taller 7.5 cm obstacle case.

As shown in Figure 7 at timestep 180, the reaction wave formed at the surface of the 11.5 cm obstacle is tall and quickly reaches the upper boundary. However, when it reflects from this upper boundary, it generates a detonation travelling upstream, but not a detonation travelling downstream. Meanwhile, the transmitted shock front that passed over the obstacle must travel a longer distance to reach the lower boundary. The transmitted shock front reflects from the lower boundary at 300 timesteps, and creates a reaction wave there, which eventually transitions to detonation at 480 timesteps. Therefore, as shown in Table II, the complete transition to detonation for the 11.5 cm obstacle occurs much later than for the other two obstacle sizes considered. The transition to detonation for the tallest obstacle occurs only as the reaction wave forms at the lower boundary, and not from a detonation front reflecting from the upper boundary. Therefore, different mechanisms are responsible for the transition to detonation for the different obstacle sizes considered. The earliest transition to detonation downstream occurs for the 7.5 cm obstacle, which provides a 50% blockage to forward flow. Reflection of the detonation front from the upper boundary and the formation of a reaction wave at the lower boundary both contribute to the rapid transition to detonation for the 50% blockage case. Although the formation of a reaction front at the lower boundary occurs earliest for the 3.5 cm obstacle (25% blockage to forward flow), reflection from the upper boundary occurs later for this obstacle blockage case, and hence transition to detonation occurs later than for the 50% blockage case. The 11.5 cm obstacle (75% blockage to forward flow) has the slowest transition to detonation downstream because the only mechanism for transition to detonation effective in this case is the formation of a reaction front at the lower boundary.

Figure 8 shows the position of the leading detonation front at timestep 400. As shown, the detonation front has travelled the farthest distance for the 7.5 cm obstacle, which provides a 50% blockage to forward flow. The position of the detonation front for the 3.5 cm obstacle case closely follows that of the 7.5 cm obstacle. For the 11.5 cm obstacle, a partial detonation front exists near the lower boundary (due to the formation of the reaction front near this boundary at 300 timesteps), however, the detonation has not yet become sufficiently strong to cover the full distance between the top and bottom boundaries; by timestep 480, this partial detonation does transition to a full detonation extending fully between the top and bottom boundaries.

Figures 9-a and 9-b show two properties of the leading shock front after it passes over the obstacle: the distance it has travelled and its velocity, both as a function of time. As discussed above, the obstacle providing a 50% blockage transitions to detonation first due to the combination of two ignition mechanisms. The maximum velocities reached by the 50% and 25% blockage cases are 2200 m/s, however, the velocity of the 50% blockage case quickly drops off to approximately 1800 m/s, while the velocity of the 25% blockage case remains at 2100 m/s for a longer period of time. Therefore, by 500 timesteps, the leading shock front in the 25% blockage case has caught up with that for the 50% blockage case, as shown in Figure 9-a. For all three obstacle sizes considered, the velocity of the detonation front asymptotically approaches 1800 m/s (Fig. 9-b), which is very close to the Chapman-Jouguet velocity, 1764 m/s, for this mixture (Gordon and McBride 1976).

Cases C-1, B-1, C-2: Effect of Incident Mach Number

To study the effect of incident Mach number on the resulting detonation, Case C simulations were conducted with incident shock Mach numbers 1.40 (Case C-1), 1.34 (Case B-1) and 1.31 (Case C-2). Temperatures in the reflected shock region are 1536 K (M = 1.40), 1350 K (M = 1.34), and 1293 K (M = 1.31). Simulations were not conducted for Mach numbers below 1.31, as the induction time was too long for spontaneous ignition to occur within the time frame considered here.

Pressure and product contours at timestep 400 for the three different incident Mach numbers are shown in Fig. 10. As the strength of the original incident shock wave is increased, the reaction wave formed at the obstacle surface is stronger and consequently transitions more quickly to a detonation travelling upstream. This trend is shown in the detonation initiation times shown in Table III. For the strongest incident shock considered, the detonation expanding

above the obstacle reflects off of the top boundary earlier and therefore results in a transition to detonation downstream earlier.

Experiments by Moen *et al.* (1982, 1986) studied the effects of an array of obstacles on the flame acceleration and transition to detonation of acetylene, propane, and hydrogen-sulfide mixtures in air. The experimental data (Moen *et al.* 1986) showed that the configuration of the obstacle array, the degree of confinement, and the strength of ignition source all have a significant effect on the potential for flame acceleration and transition to detonation. Although the conditions of this experiment are considerably different from those of the numerical simulation so that they cannot be directly compared, the trends observed in the experiments are similar with those observed in the simulations. The experimental data showed that under certain conditions, the propane and hydrogen-sulfide mixtures in air would not transition to detonation; however, stronger ignition sources or more confinement would cause these mixtures to transition to detonation. The simulations show that the stronger ignition sources result in earlier transition to detonation, and that for incident shocks below Mach 1.31, ignition would not occur at all within the time frames considered here.

More direct comparisons of experiment and simulations can be made with the experimental work of Teodorczyk *et al.* (1988), in which Schlieren photographs provide detailed views of the propagation of quasi-detonations in a stoichiometric propane-oxygen mixture. The experimental apparatus was a rectangular channel 6.1 cm high x 6.1 cm wide x 150 cm long, containing obstacles of height 2.54 cm. The experimental results show that the propagation velocity increases as the unobstructed passage distance (distance between top of obstacle and upper boundary wall) increases. They observed that the obstacles play a negative role in the wave propagation by attenuating the detonation by diffraction. The numerical simulations

Table III. Time of transition to detonation as a function of incident shock Mach number.

Mach number	Time of transition to detonation (timesteps)
1.40	300
1.34	320
1.31	420

presented here (Figures 9-a and 9-b) also show that the propagation velocity (before asymptotically approaching the Chapman-Jouguet velocity) is greatest for the smallest obstacle. Similarly, the tallest obstacle significantly attenuated the detonation, resulting in much lower initial propagation velocities.

The experiments of Teodorczyk *et al.* (1988) also showed that ignition occurred when the transmitted wave reflects off of the lower and upper boundaries of their channel. Using wire screens to effectively damp out shock reflections, they observed that transition to detonation is greatly delayed when shock reflections are not permitted, and so provided experimental evidence of the important role of shock reflections to the transition to detonation. This phenomenon is shown in the simulations presented here. In fact, all of the mechanisms for transition to detonation displayed in the numerical simulations occur in the experiments; the simulations allow these mechanisms to be studied in more detail.

Case D: Variable Stoichiometry Around the Obstacle

For Case D, the inflowing gas was air while the background gas was a propane-air mixture of variable stoichiometry. This scenario simulates a situation where the fuel has leaked from the storage container. As shown in Fig. 11, the mixture is fuel-rich ($\phi = 2$) in the area surrounding the obstacle, and the equivalence ratio decreases linearly with distance from the obstacle such that the mixture is fuel lean $\phi = 0.5$ at the boundaries of the simulated volume.

Figure 12 shows the pressure and product contours for timesteps 180 through 420. When the incident shock wave approaches the obstacle, the fuel is compressed and heated at the face of the obstacle and ignition occurs here. However, reaction does not proceed very far upstream because the air (from the incident shock) has displaced much of the fuel. Hence, the reaction in the reflected shock region is confined to the area near the face of the obstacle. The reflected shock continues to move upstream and expand upwards into the region above the obstacle and reaches the top boundary in approximately 200 timesteps. However, the location where the shock reflects off of the wall is in a fuel-rich region, where chemical induction times are too long for ignition to occur. Therefore, we do not see the formation of products when the shock wave reflects off of the upper wall boundary. This variable stoichiometry case differs considerably from the stoichiometric case (Case B-1) where the reaction in the reflected shock region (at the face of the obstacle) quickly transitions to a detonation which travels upstream and expands above the obstacle, and then reflects off of the upper wall boundary producing a detonation travelling upstream and downstream.

When the original incident shock reflects off of the obstacle, the expansion over the obstacle and flow behind the reflected shock allows a considerable amount of hot products to be driven over the obstacle, causing the same kinds of shedding and vortex patterns seen with the stoichiometric case (Case B-1). Starting at timestep 340, ignition occurs downstream from the obstacle due to the mixing of hot products with unreacted fuel in this turbulent shear layer, and helped by the reflection of the very weak transmitted shock wave off of the lower wall boundary. This ignition source develops into a reaction front which travels upstream and downstream to consume unreacted fuel.

Figure 13 shows pressure, product and equivalence ratio (ϕ) contours at timesteps 460 to 580. At timestep 460, a second point of ignition occurs downstream when the transmitted shock front enters the region of $\phi \sim 1.2$. The ignition occurs here because the transmitted shock has reflected off of the lower boundary, creating a triple point at this location where the mixture is approaching stoichiometric proportions. The ignition occurs behind this triple point due to adiabatic heating near a Mach stem, an effect that has been observed in experiments (Teodorczyk *et al.* 1988) and simulations (Oran *et al.* 1990). The second ignition point develops into a reaction wave which moves upstream (timesteps 500-560) and merges with the first reaction wave (by timestep 580) and also moves downstream. The reaction wave moving downstream eventually overtakes the transmitted shock and transitions to a detonation.

However, as this detonation continues to move into the area of decreasing fuel concentration ($\phi < 1$), it decays into a separate flame and shock front. Figure 14 shows temperature profiles at timesteps 780 through 880. At timestep 780, the shock front and reaction front have merged and transitioned to a detonation, as shown by the steep contour at timestep 780. However, by timestep 820, the two fronts have begun to separate and continue to separate further with time as the leading shock front is transmitted through a mixture of progressively leaner fuel concentration.

Resolution tests were conducted on this variable-stoichiometry case to determine if the grid used provided adequate resolution of the structure between the reaction and shock fronts. A comparison between the standard (200 x 30) grid and for one with exactly double the resolution is shown in Figure 15, which shows pressure, density, product and fuel concentration contours at time 5.76×10^{-4} s. This time corresponds to 500 timesteps for the standard grid, but to 1000 timesteps for the more resolved grid, since the timestep is halved when the grid resolution is doubled. Figure 15 shows that the less resolved simulation is more numerically diffusive, as would be expected. However, the basic quantitative and qualitative features of the

two simulations are very similar. The most obvious differences between the simulations are in the sharpness and resolution of the structures formed from the shedding from the obstacle. Neither of these simulations are properly resolving all of the scales that are likely to be generated by such a complex flow, although the basic features seem to be captured. However, the comparison shows that the simulations do resolve the detonation and reignition adequately.

5. SUMMARY AND DISCUSSION

We have used a solution of the reactive flow conservation equations to describe the spontaneous ignition and subsequent transition to detonation of various propane-air mixtures after a weak planar shock reflects from an obstacle that is leaking propane gas. The numerical model consists of the two-dimensional solution of the fully compressible equations for conservation of density, momentum, and energy (Boris and Book 1976, Oran and Boris 1987, Boris *et al.* 1992) coupled to a model for species conversion and energy release based on the induction parameter model originally introduced by Oran *et al.* (1981) and further developed by Kailasanath *et al.* (1985). In the case considered here, the input data for this model are taken from the summary of experimental data by Burcat *et al.* (1971). A new feature of this implementation is the use of a model to treat ignition of a propane-air mixture in a gas with variable stoichiometry.

The first problem considered was a shock hitting an obstacle completely surrounded with a stoichiometric propane-air mixture. If the obstacle were not present, the elevated temperature caused by the incident planar shock would not be high enough to cause ignition in the reactive gas within the time frame considered in these simulations. Typical temperatures behind the incident shocks considered here are on the order of 800 K and pressures were on the order of 9×10^6 dynes/cm^2, which correspond to a spontaneous ignition time of approximately 5 seconds.

The presence of the obstacle changed the flow structure such that shock-heated regions and turbulent mixing caused a series of ignition centers. The first ignition source was behind the shock reflection from the obstacle itself, and this caused a detonation that propagated upstream. When this first detonation reflected from the top boundary above the obstacle, it created a second detonation which moved downstream and eventually caught up with the original transmitted shock. This second detonation was attached to a curved shock that propagated down into reacted material, but finally reached a region of turbulent, unreacted material which then ignited either immediately (due to heating in the vortical structures) or due to another shock reflection from the lower boundary. The combination of these three ignition sources finally resulted in two propagating detonations, one moving upstream and one moving downstream, and

these continue until all of the unreacted material is consumed.

A series of computations performed to evaluate the effect of changing the relative height of the obstacle showed that obstacle size had a dramatic effect on the type of mechanism involved in the transition to detonation. For short obstacles, a reaction wave quickly formed at the lower boundary, however, it took longer for the detonation (expanding in the region above the obstacle) to reflect from the top wall. For the tall obstacle, the detonation expanding in the region above the obstacle quickly reflected from the top boundary, but it only generated a detonation travelling upstream. A reaction wave formed when the transmitted shock reflected off of the lower boundary, and this did eventually transition to detonation, but took considerably more time than for the shorter obstacle cases. The transition to detonation occurred most rapidly for the case of 50% flow blockage by an obstacle, because the effect of both the reaction wave at the lower boundary and the reflection of the detonation from the top boundary contributed to the quick transition to detonation.

Several incident shock strengths were considered in the range from Mach 1.31 to Mach 1.40. Transition to detonation occurred for all of the incident shock strengths in this range, it simply took longer for the transition to detonation to occur as the ignition strength decreased. Incident shocks with Mach numbers less than 1.31 were not considered because the reflected shock temperature was too low to cause spontaneous ignition in the reflected region within the time frame considered here.

A simulation with variable stoichiometry represented a scenario where the propane mixture leaked from the storage container, but did not diffuse evenly throughout the entire volume simulated. Hence the fuel concentration was greatest near the container and proportionately decreased with distance from the container. This computation showed some of the same flow and ignition properties we saw in the stoichiometric case, but there were some notable differences. First, there was some product formed after the original shock reflected from the obstacle, but this did not result in an upstream-propagating detonation since most of the fuel was driven over the obstacle by the incident shock. The result was then a shock, rather than a detonation, propagating upstream. When this shock reflected from the top boundary, it formed a reflected shock, rather than a combined shock-detonation structure as seen in the stoichiometric case, again for reasons of mixture composition.

There were, however, two separate ignition sources downstream of the obstacle. The first ignition source occurred in the turbulent mixture caused as the flow passed over the obstacle, and this turbulent region was further heated by the reflected shock travelling down from the

upper boundary. The second ignition source was in the region of the Mach stem formed as the original transmitted shock reached a stoichiometric region further downstream. These two ignition sources merged to form a detonation, but this detonation decayed as it propagated into a fuel-lean region.

The standard grid used in the simulations was a 200 x 30 cell uniform grid. Resolution tests were conducted by comparing computations on the standard, admittedly rather coarse grid to computations on a grid twice as resolved. In particular, we have shown results from the case with variable stoichiometry. These tests showed that the standard (less resolved) grid case was indeed more numerically diffusive, however, the basic features of the ignition and the detonation transition processes were very similar for both grids. The simulation with the finer grid did, however, show sharper structures in the region of the complex shedding patterns that developed from the flow around the obstacle, and with an even finer grid, it is likely that more structure would result. However, the increased resolution did not provide any additional or different quantitative or qualitative results about the ignition mechanisms. We thus believe that a further increase in resolution would not be necessary to study the general features of the process, although there are features of the flow that could benefit from more resolution, such as the details of the ignition in the vortices and Mach stems.

The obstacle represented in the two-dimensional simulations was a simple rectangle. Simulations conducted in three dimensions, where the obstacle could, for example, be represented by a parallelepiped, would have shown even more complex flow structure. We would expect ignition to occur initially as the shock wave reflects off of the cube surface that is normal to the incident shock wave, which is similar to what we have seen here in two dimensions. Again, a complex vortex shedding pattern would result, mixing hot product and unreacted cold fuel. A weakened transmitted shock would reflect off the various wall boundaries. Quantification of these speculations, however, can only be done by experiments or more extensive three-dimensional simulations.

NOMENCLATURE

A_r	pre-exponential factor
E_r	activation energy
E	total energy density
f	fraction of chemical induction time elapsed
k	Boltzmann constant
M	Mach number
L_i	chemical loss term
n_i	individual species number densities
N	total species number density
N_s	total number of kinds of species present
P	pressure
Q_i	chemical production term
R	mixture gas constant
T	fluid temperature
t	time
$\bar{v}$	fluid velocity
ρ	fluid mass density
e	specific internal energy
γ	ratio of specific heats
τ_i	chemical induction time
ϕ	equivalence ratio

ACKNOWLEDGEMENTS

This work was sponsored by the Naval Research Laboratory through the Office of Naval Research. The authors would like to thank Dr. K. Kailasanath for helpful discussions while implementing the chemical induction model, and Drs. F. Williams, P. Tatem, and J. Boris for providing the resources and environment necessary for this work to be accomplished.

REFERENCES

Boris, J.P. and Book, D.L. (1976). Solution of the Continuity Equation by the Method of Flux-Corrected Transport. *Methods in Computational Physics*, **16**, 85.

Boris, J.P., Gardner, J.H., Oran, E.S., Zalesak, S., Ellzey, J., Patnaik, G. Book, D.L., Guirguis, R.H. (1992). *LCPFCT - A Monotone Algorithm for Solving Continuity Equations*, Naval Research Laboratory Memorandum Report (to appear).

Burcat, A., Lifshitz, A., Scheller, K., Skinner, G.B. (1971). Shock Tube Investigation of Ignition in Propane-Oxygen Argon Mixtures. *Proceedings of the Thirteenth Symposium (International) on Combustion*, The Combustion Institute, Pittsburgh, PA., p. 745.

Chan, C., Moen, I.O. and Lee, J.H.S. (1983). Influence of Confinement on Flame Acceleration Due to Repeated Obstacles. *Combust. Flame*, **49**, 27.

Gordon, S. and McBride, B.J. (1976). *Computer Program for Calculation of Complex Chemical Equilibrium Compositions, Rocket Performance, Incident and Reflected Shocks, and Chapman-Jouguet Detonations*, NASA Report SP-273, National Aeronautics and Space Administration.

Guirguis, R., Oran, E.S., and Kailasanath, K. (1986). Numerical Simulatons of the Cellular Structure of Detonations in Liquid Nitromethane - Regularity of the Cell Structure. *Combust. Flame*, **65**, 339.

Guirguis, R., Oran, E.S., and Kailasanath, K. (1987). The Effect of Energy Release on the Regularity of Detonation Cells in Liquid Nitromethane. *Proceedings of the Twenty-First Symposium (International) on Combustion*, The Combustion Institute, Pittsburgh, PA 11987, p. 1659.

Hjertager, B.H. (1982). Simulation of Transient Compressible Turbulent Reactive Flows. *Comb. Sci. Tech.*, **27**, 159.

Kailasanath, K., Oran, E.S., and Boris, J.P. (1985). Determination of Detonation Cell Size and the Role of Transverse Waves in Two-Dimensional Detonations. *Combust. Flame*, **61**, 199.

Kaplan, C.R. and Oran, E.S. (1991-a). A Numerical Study of Spontaneous Ignition in a Partially Confined Volume. *Fire Safety Science: Proceedings of the Third International Symposium*, p. 375, eds. G. Cox and B. Langford, Edinburgh, Scotland, U.K.

Kaplan, C.R. and Oran, E.S. (1991-b). Mechanisms of Ignition and Detonation Formation in Propane-Air Mixtures, *Comb. Sci. Tech.*, **80**, 185.

Moen, I.O. and Sulmistras, A. (1986). Flame Acceleration and Transition to Detonation in Large Fuel-Air Clouds with Obstacles. *Defense Research Establishment Suffield Memorandum No. 1159*, Ralston, Alberta, Canada.

Moen, I.O., Bjerketvedt, D., Jenssen, A., and Thibault, P.A. (1985). Transition to Detonation in a Large Fuel-Air Cloud. *Combust. Flame*, **61**, 285.

Moen, I.O., Sulmistras, A., Hjertager, B.H., and Bakke, J.R. (1986). Turbulent Flame Propagation and Transition to Detonation In Large Fuel-Air Clouds. *Proceedings of the Twenty-First Symposium (International) on Combustion*, The Combustion Institute, Pittsburgh, PA, p. 1617.

Moen, I.O., Lee, J.H.S., Hjertager, B.H., Fuhre, K., and Eckhoff, R.K. (1982). Pressure Development Due to Turbulent Flame Propagation in Large-Scale Methane-Air Explosions. *Combust. Flame*, **47**, 31.

Oran, E.S., Boris, J.P., Young, T.R. and Picone, J.M. (1981). Numerical Simulations of Detonations in Hydrogen-Air and Methane-Air Mixtures. *Proceedings of the Eighteenth Symposium (International) on Combustion*, The Combustion Institute, Pittsburgh, PA, p. 1641.

Oran, E.S. and Boris, J.P. (1987). *Numerical Simulation of Reactive Flow*, Elsevier, New York, NY.

Oran, E.S., Jones, D.A., and Sichel, M. (1990). The Anatomy of a Marginal Detonation. *Proceedings of the Royal Society* (submitted).

Taylor, P.H. (1986). Fast Flames In a Vented Duct. *Proceedings of the Twenty-First Symposium (International) on Combustion*, The Combustion Institute, Pittsburgh, PA., p. 1601.

Teodorczyk, A., Lee, J.H.S., and Knystautas, R. (1988). Propagation Mechanism of Quasi-Detonations. *Proceedings of the Twenty-Second Symposium (International) on Combustion*, The Combustion Institue, Pittsburgh, PA 11987, p. 1723.

Urtiew, P.A., Brandeis, J. and Hogan, W.J. (1983). Experimental Study of Flame Propagation in Semiconfined Geometries with Obstacles. *Combust. Sci. Tech.*, **30**, 105.

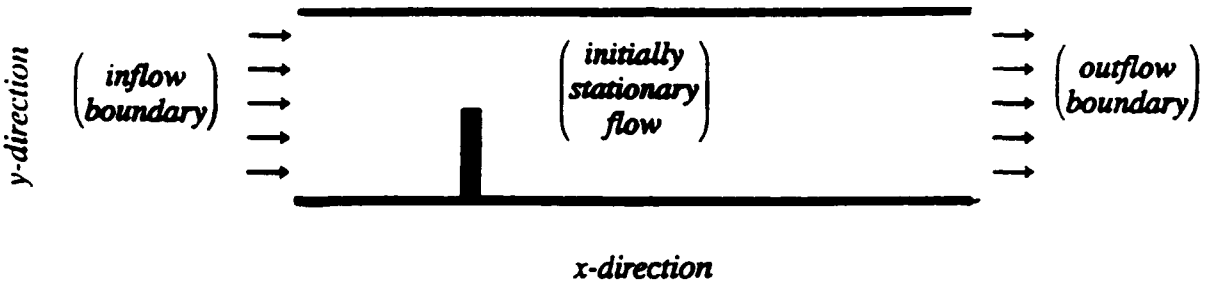

Figure 1. Computational domain. Inflow boundary condition on left-hand side, outflow boundary condition on right-hand side. Top and bottom surfaces are solid walls. The solid vertical rectangle represents the obstacle.

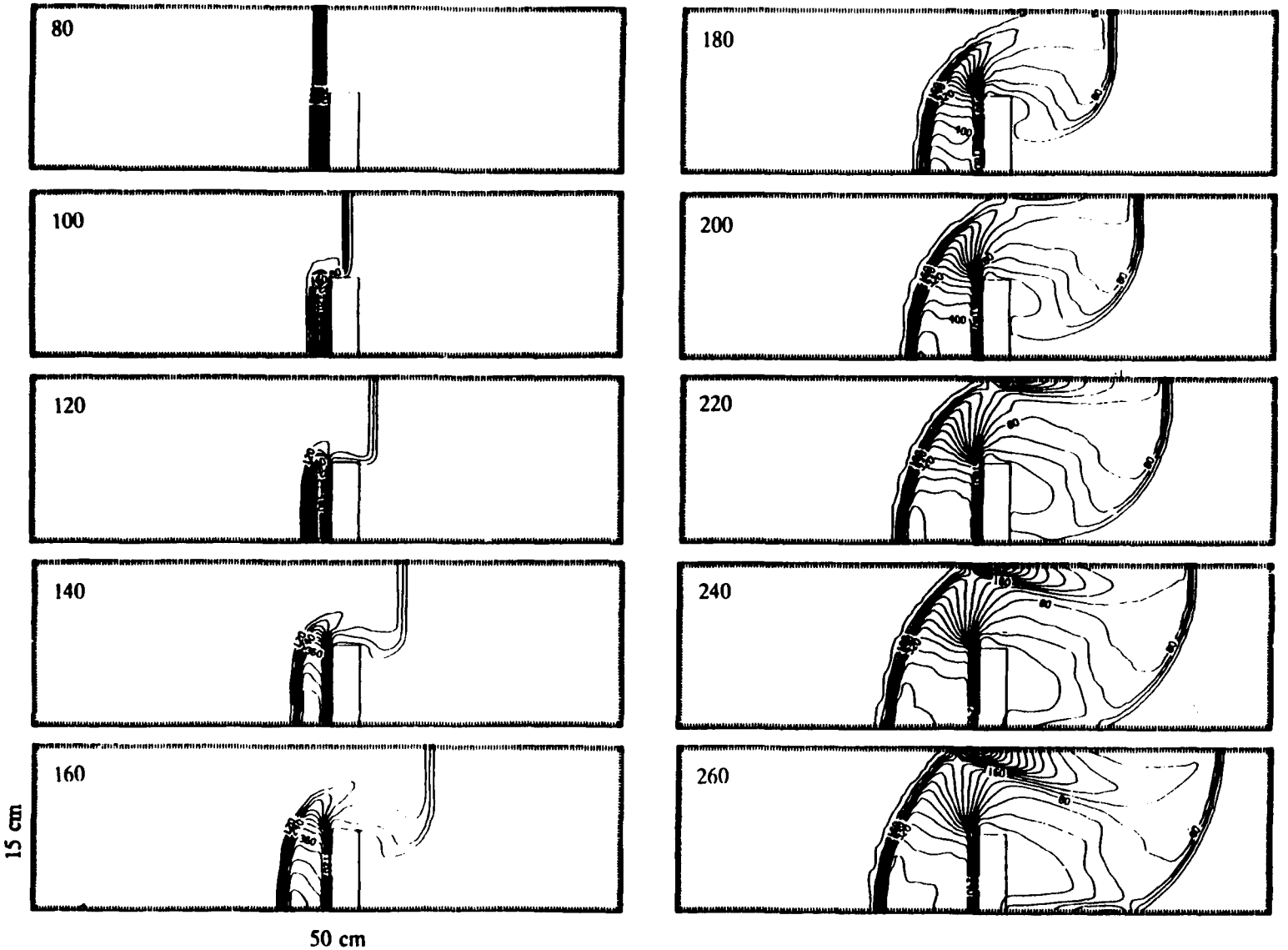

Figure 2. Pressure contours for nonreactive (air) simulation (Case A), timesteps 80-260. Contour labels are 10^5 dynes/cm^2.

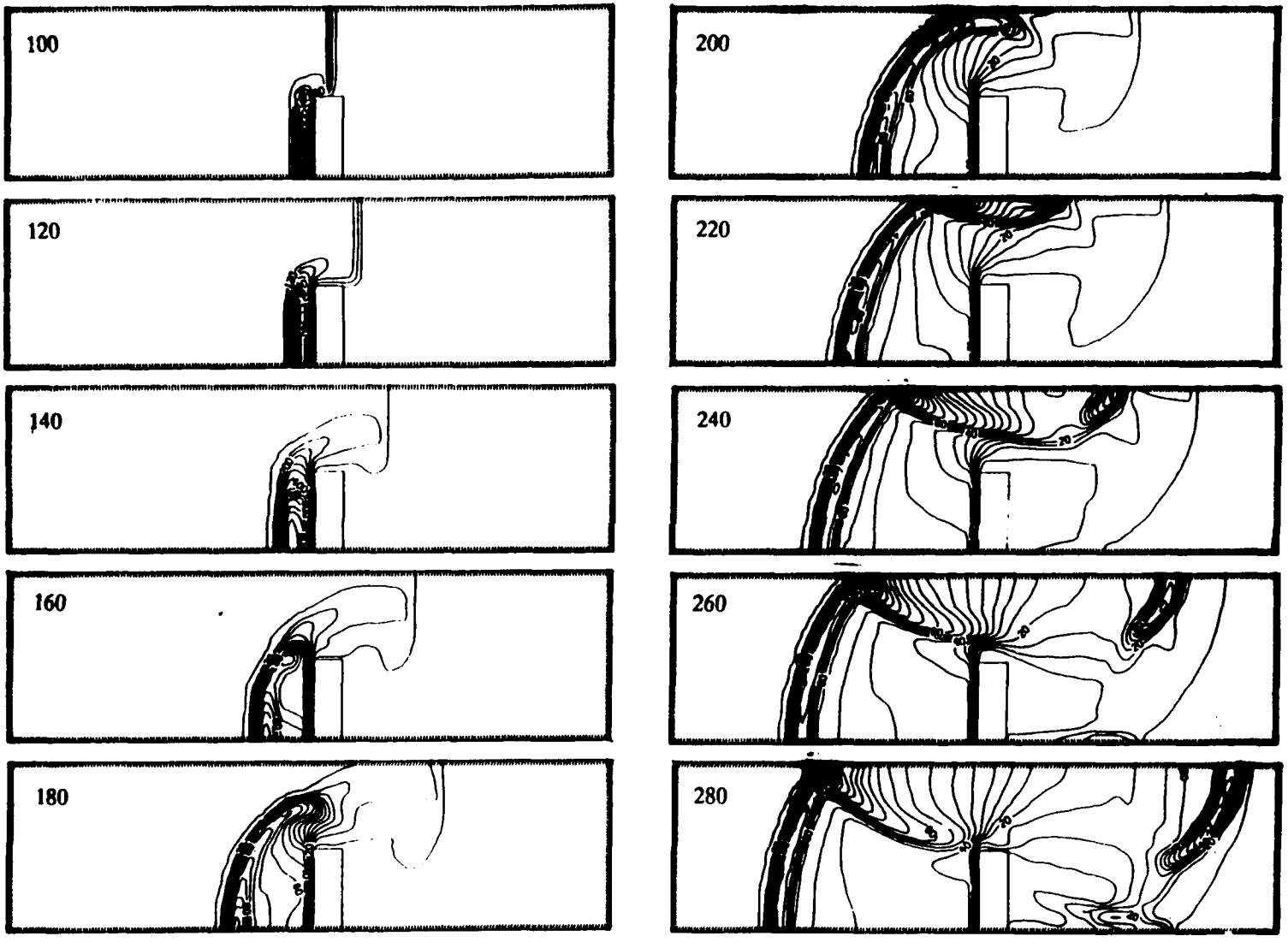

Figure 3. Pressure contours (10^6 dynes/cm^2) for stoichiometric propane-air simulation (Case B-1), timesteps 100-280.

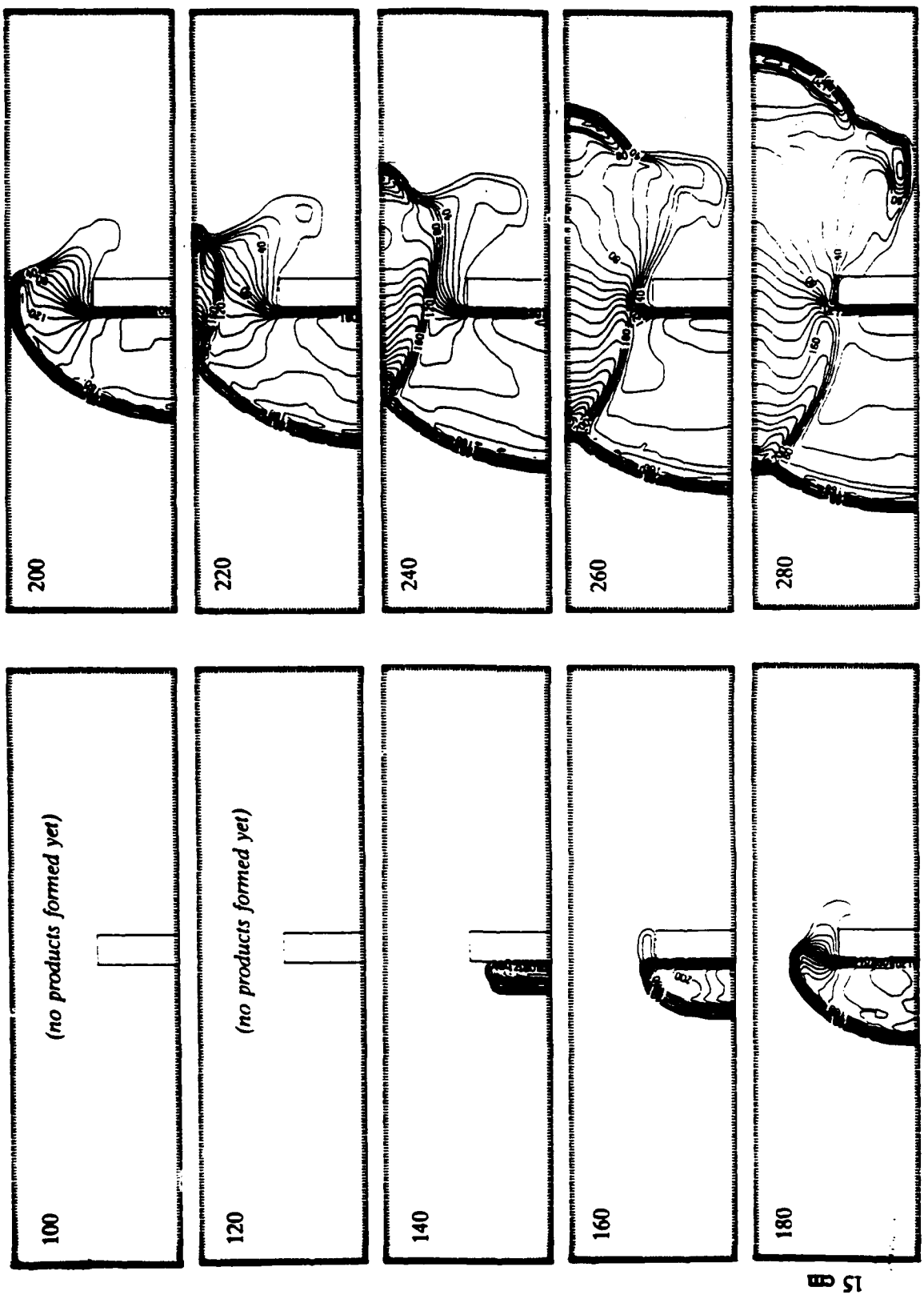

Figure 4. Product concentration contours (10^{-6} g/cm^3) for stoichiometric propane-air simulation (Case B-1), timesteps 100-280.

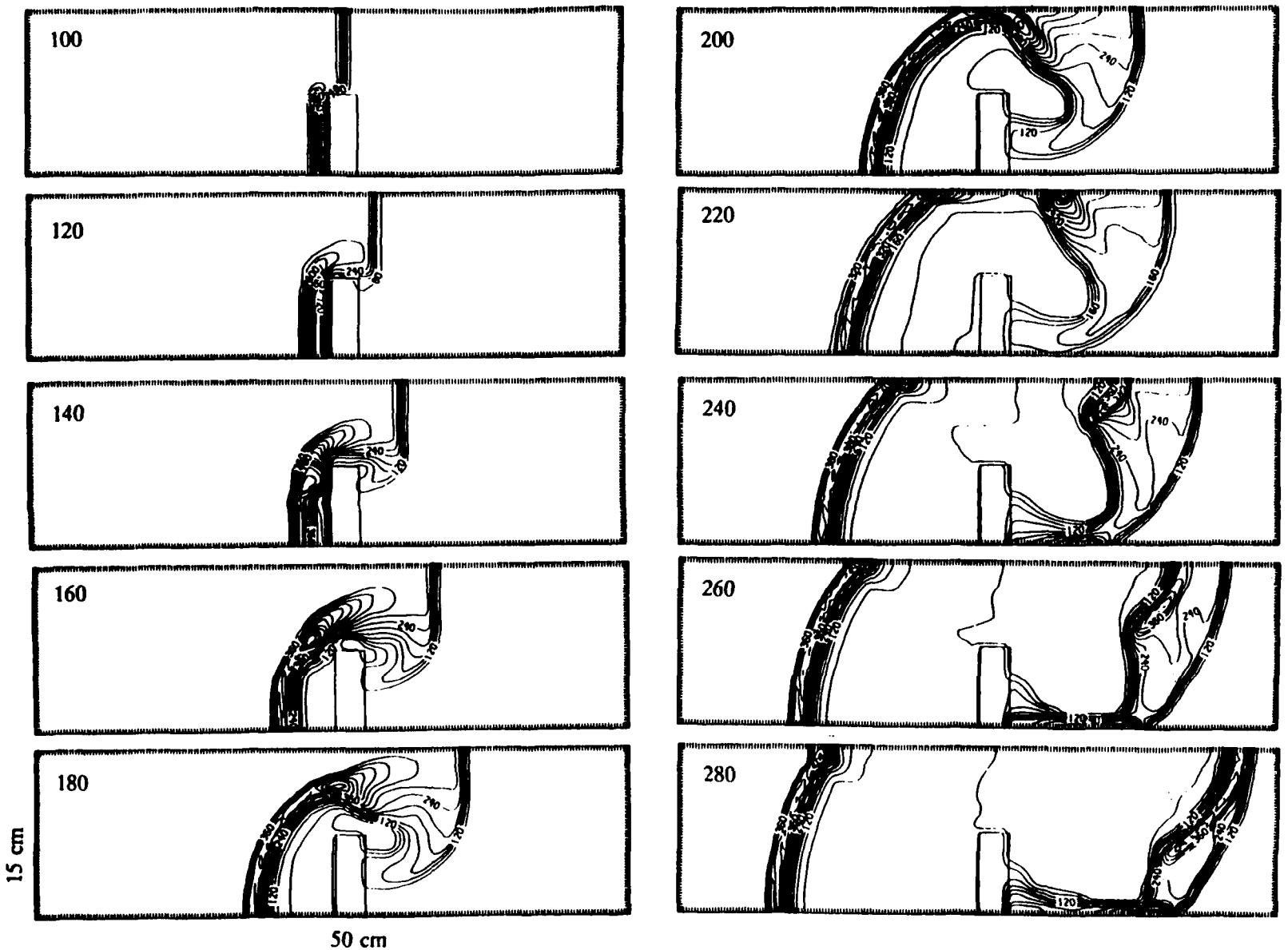

Figure 5. Fuel concentration contours (10^{-6} g/cm^3) for stoichiometric propane-air simulation (Case B-1), timesteps 100-280.

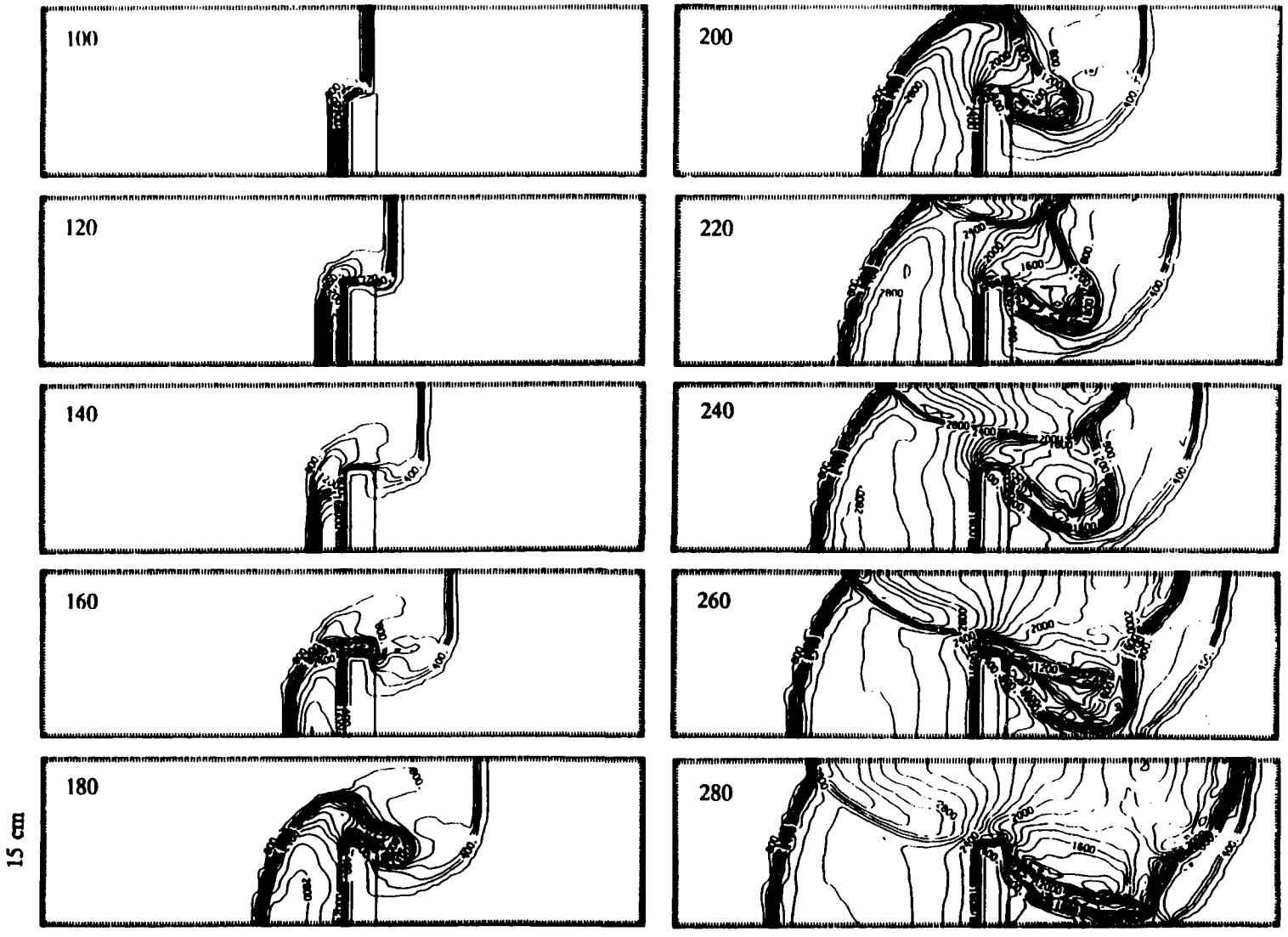

Figure 6. Temperature (°K) contours for stoichiometric propane-air simulation (Case B-1), timesteps 100-280.

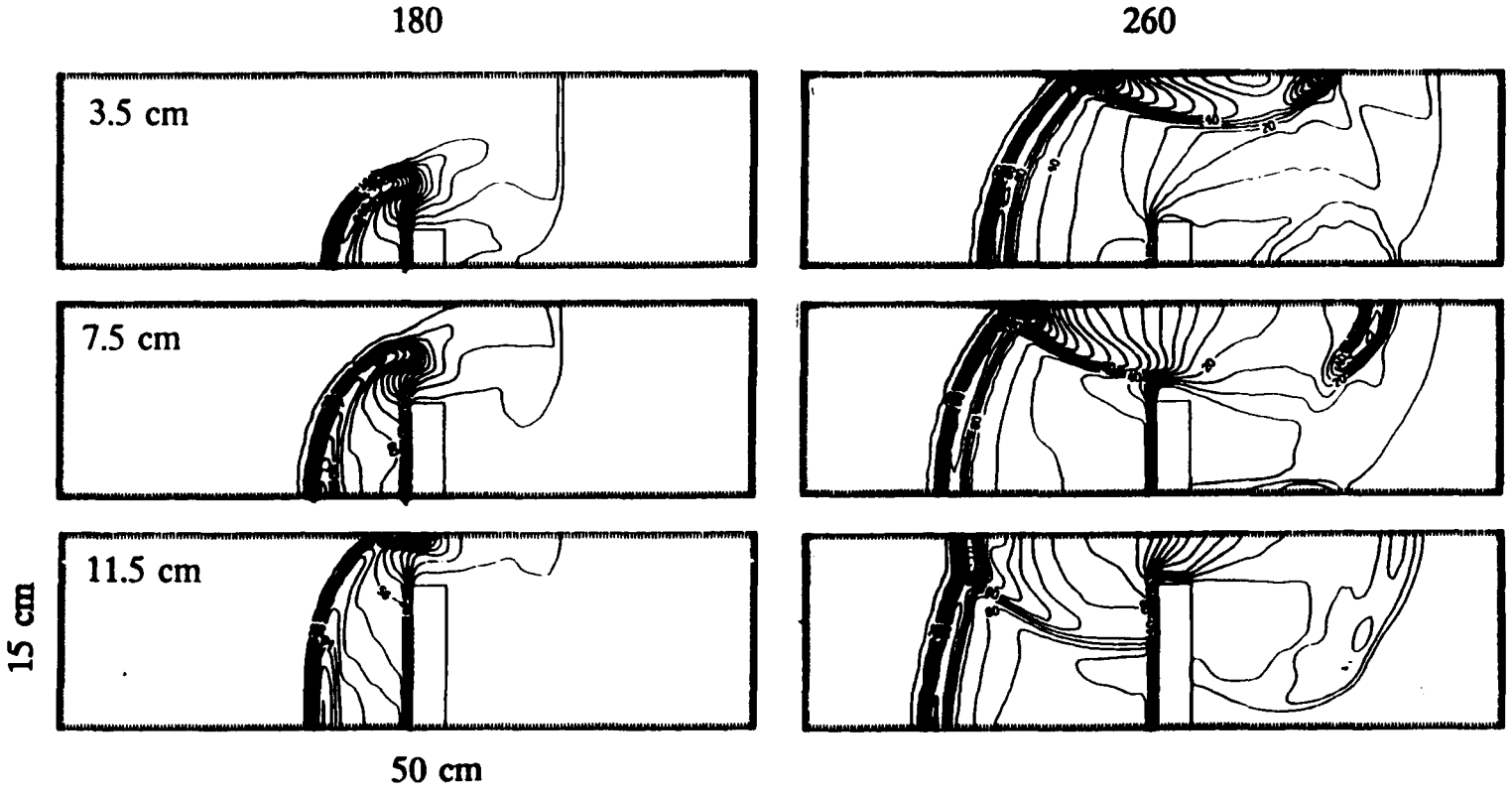

Figure 7. Pressure (10^6 dynes/cm^2) contours for stoichiometric propane-air simulation (Case B-1) at timestep 180 and 260, for obstacles of height 3.5, 7.5, and 11.5 cm.

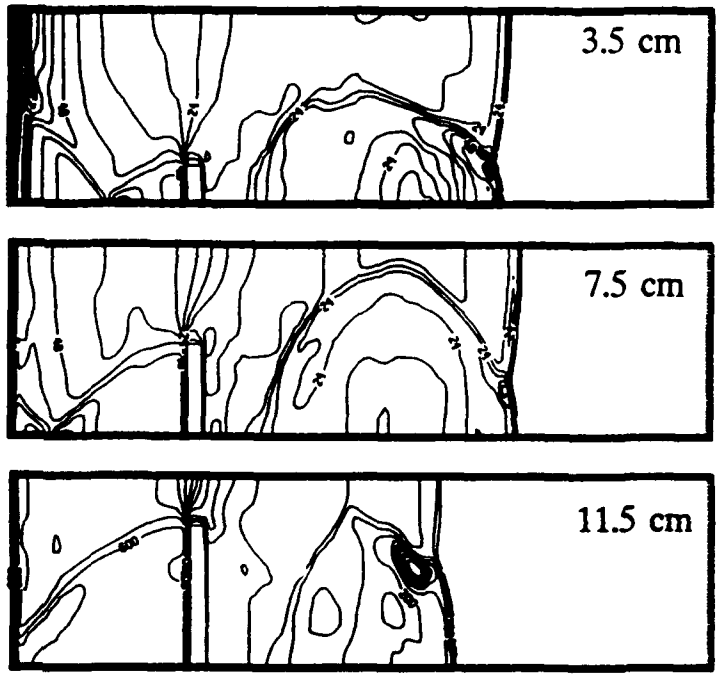

Figure 8. Pressure (10^6 dynes/cm^2) contours showing position of detonation front at 400 timesteps for obstacles of height 3.5, 7.5 and 11.5 cm for stoichiometric propane-air simulation (Case B-1).

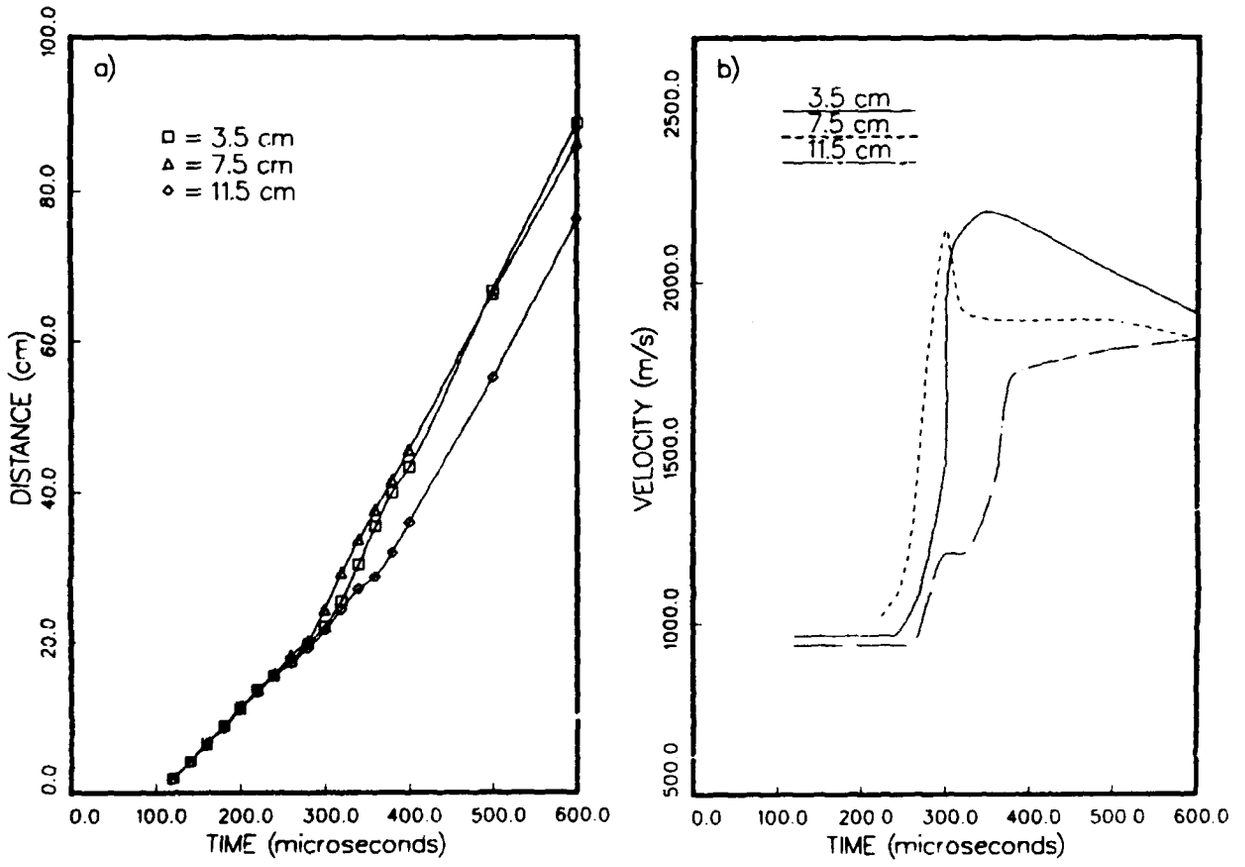

Figure 9. Distance travelled by (cm) and velocity (m/s) of leading shock front as a function of time for 3.5, 7.5 and 11.5 cm obstacles for stoichiometric propane-air simulation (Case B-1).

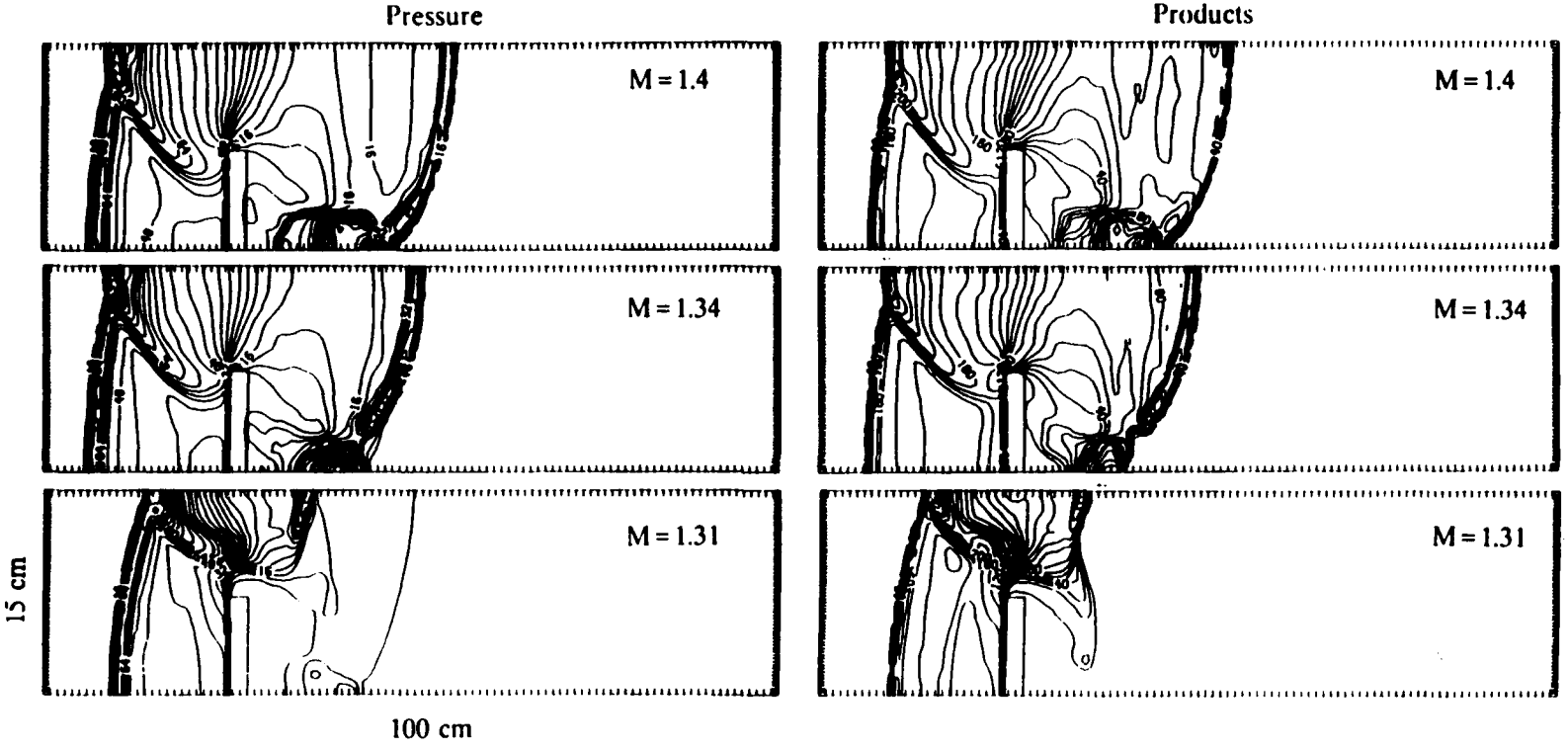

Figure 10. Pressure (10^6 dynes/cm^2) and product contours (10^{-6} g/cm^3) of simulations for incident shock waves of Mach number 1.4, 1.34, and 1.31 for stoichiometric propane-air simulation (Cases C-1, B-1 and C-2).

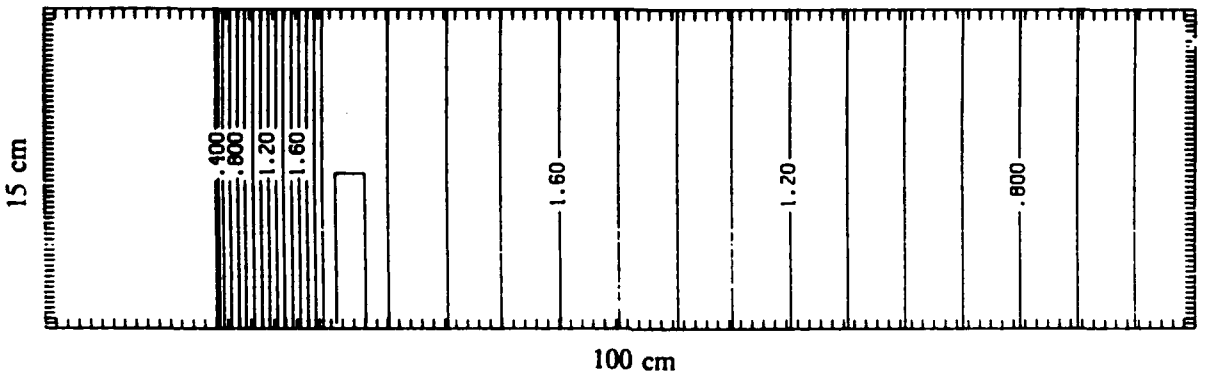

Figure 11. Equivalence ratio of propane-air mixture at the start of the variable stoichiometry simulations. Conditions are fuel-rich (ϕ-2) near the obstacle and progressively more fuel lean with distance from the obstacle.

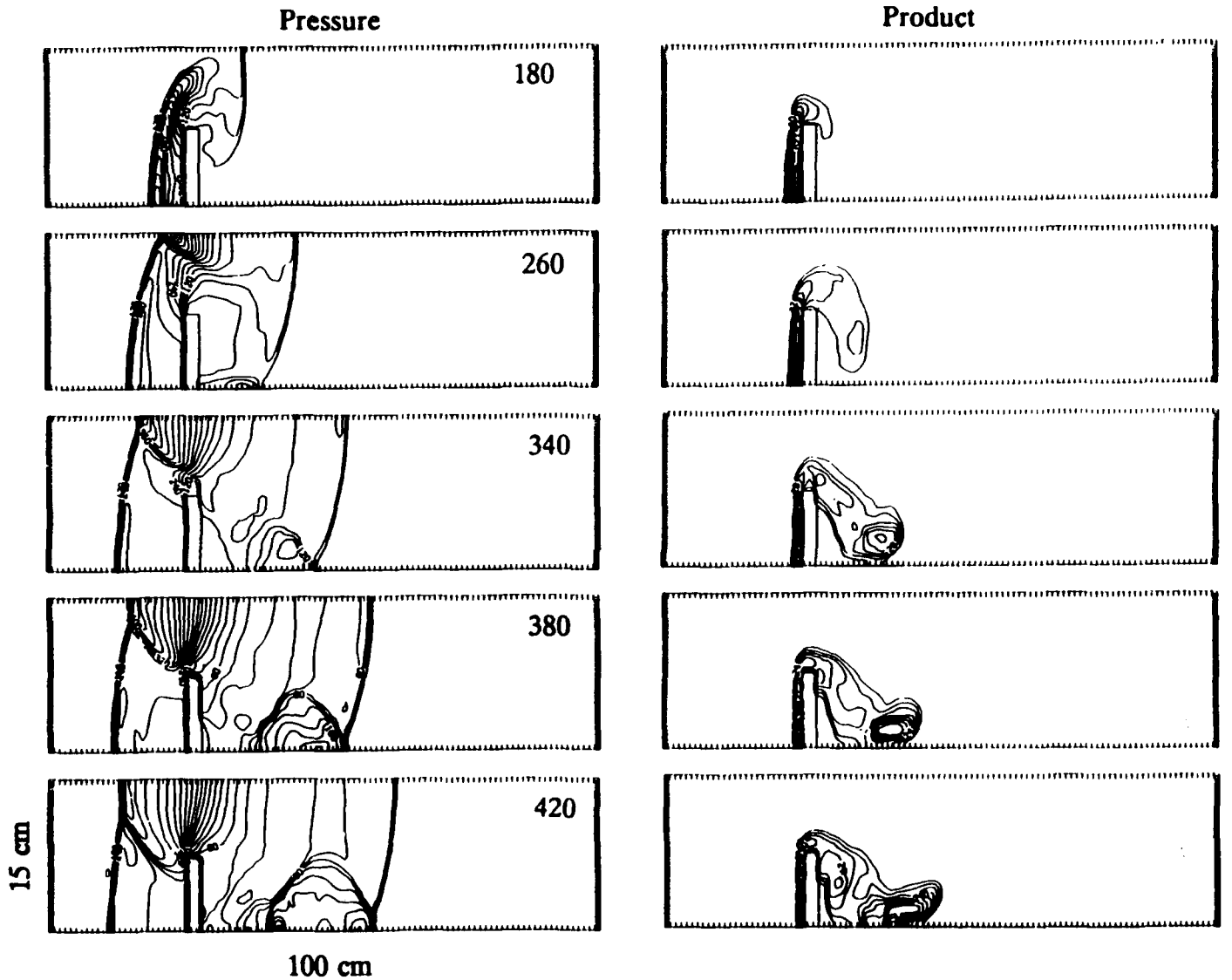

Figure 12. Pressure (10^5 dynes/cm^2) and product (10^{-5} g/cm^3) contours for variable stoichiometry (Case D) simulation, timesteps 180-420.

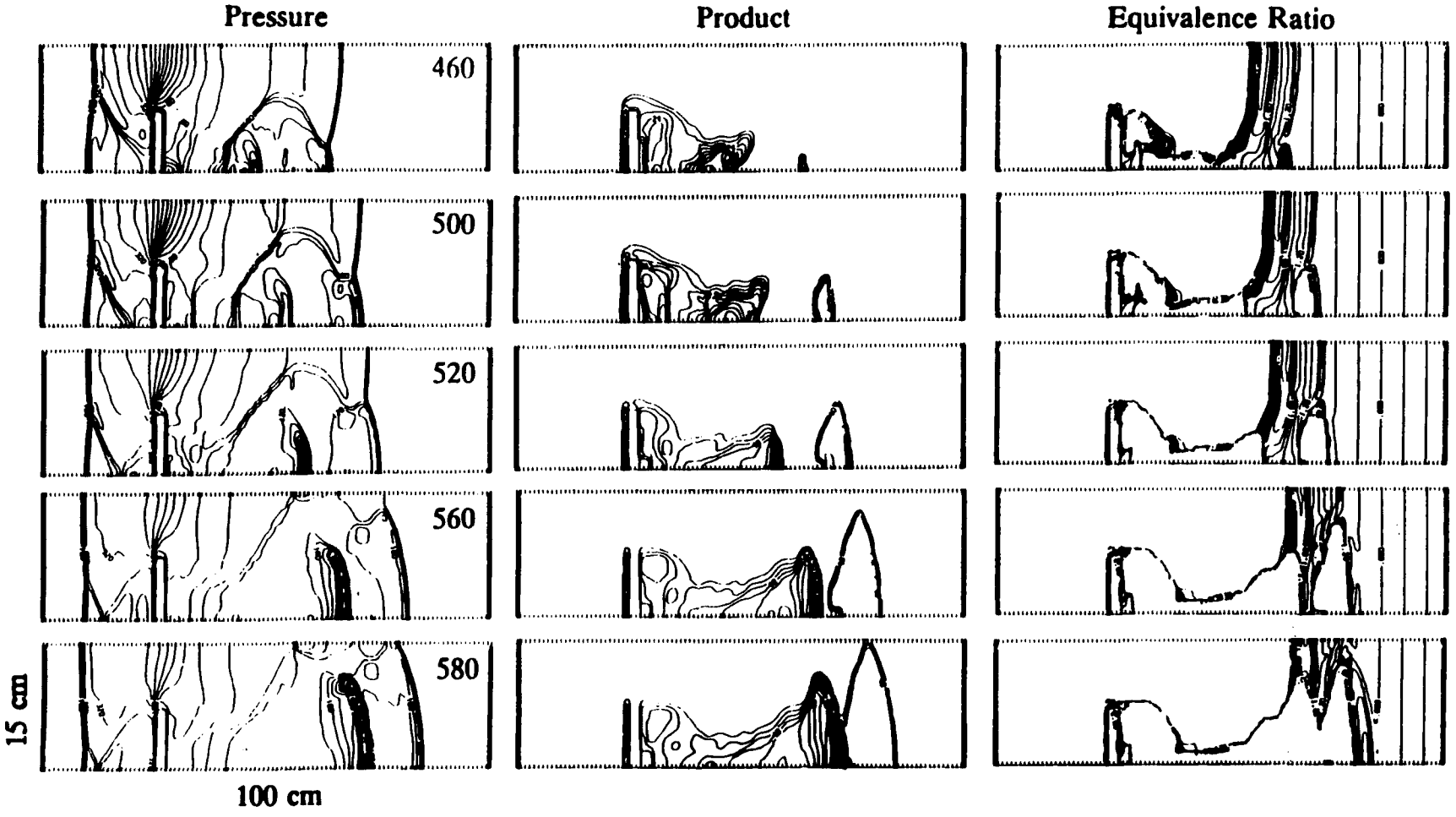

Figure 13. Pressure (10^5 dynes/cm^2), product (10^{-5} g/cm^3), and equivalence ratio(ϕ) contours for variable stoichiometry (Case D) simulation, timesteps 460-580.

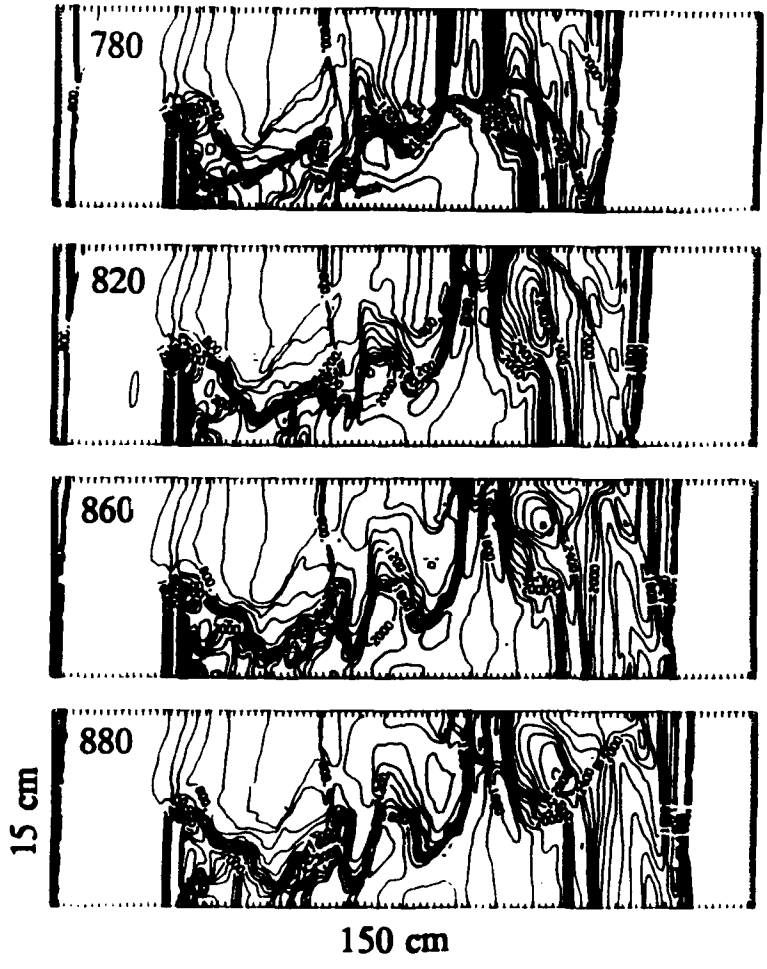

Figure 14. Temperature (°K) contours for variable stoichimetry (Case D) simulation, timesteps 780-880.

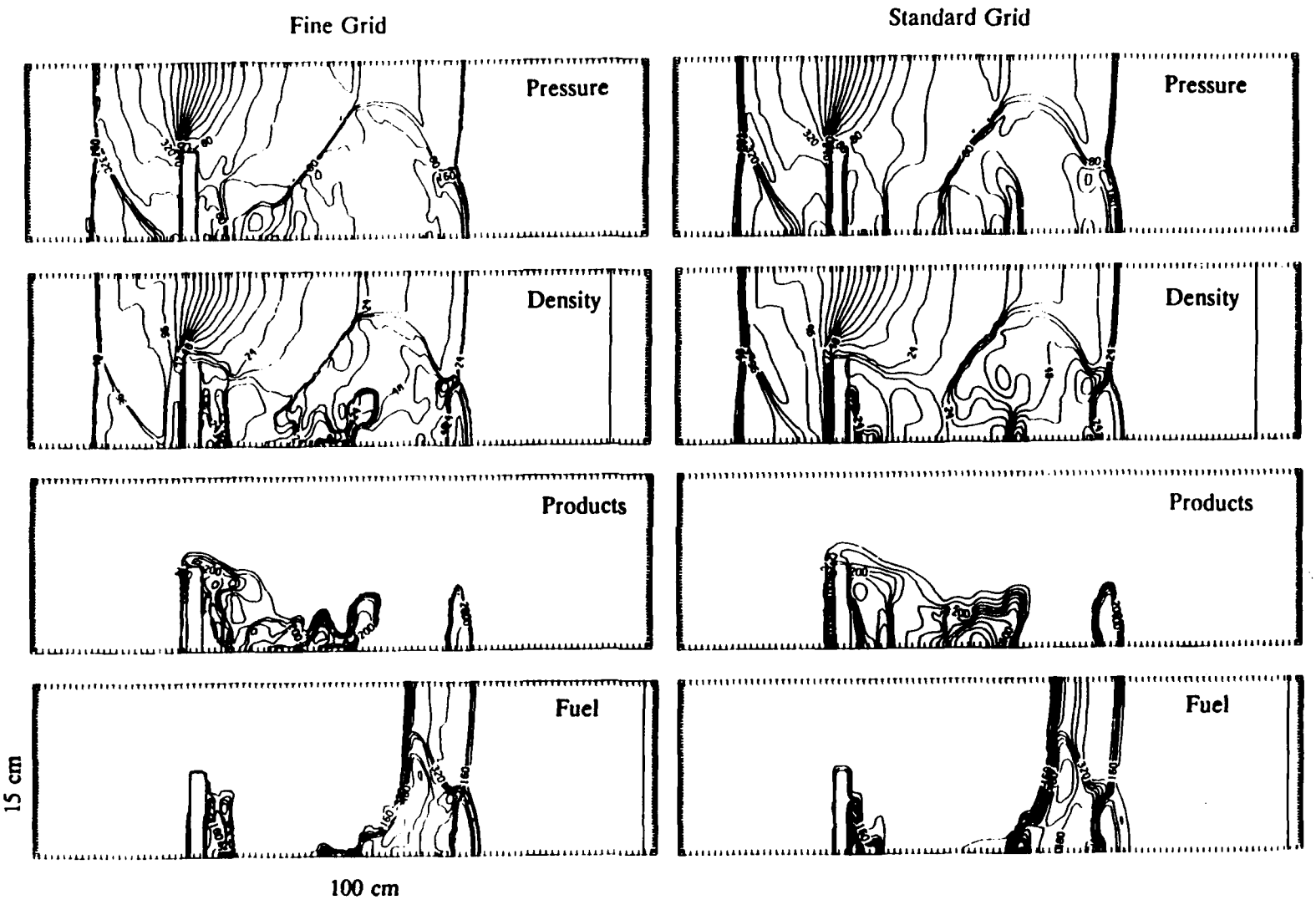

Figure 15. Resolution tests: Product concentration (10^{-6} g/cm^3), density (10^{-4} g/cm^3), pressure (10^5 dynes/cm^2) and fuel concentration (10^{-6} g/cm^3) contours for fine and standard grids at 5.76 x 10^{-4} s.